AIAA JOURNAL
Vol. 63, No. 11, November 2025

Laboratory-Scale Experiment to Study *N*-Wave Propagation into a Shadow Zone with Turbulence

Édouard Salze,* Sébastien Ollivier,† Emmanuel Jondeau,† and Philippe Blanc-Benon‡
CNRS, Ecole Centrale de Lyon, INSA Lyon, Universite Claude Bernard Lyon 1, LMFA, UMR5509, 69130, Ecully, France

https://doi.org/10.2514/1.J065049

The propagation of spark-generated *N*-waves through thermal turbulence into an acoustical shadow zone is experimentally studied at the laboratory scale into a shadow zone obtained using a curved surface. Thousands of waveforms are recorded in different regions, including the shadow zone. Statistics are described using a generalized gamma distribution. In the illuminated zone, an excellent agreement is obtained with previously published data. On average, in the illuminated zone, thermal turbulence attenuates the peak pressure by a factor of approximately 0.8, with random amplification or attenuation. Without turbulence, the pressure level rapidly vanishes in the shadow zone. Waveforms are well described using the linear analytical solution. With turbulence, a systematic amplification of the peak pressure by a factor of up to 8 is observed in the shadow zone, which is not the case in the illuminated zone. A doubling of the pressure level is a common event, with a probability of about 70%. With turbulence, the shadow zone is dominated by pressure waves previously scattered from the illuminated zone by turbulence. An increase in the surface area of maximum sound exposure is therefore observed.

I. Introduction

THE study detailed here presents an experiment and discusses results on the effects of turbulence on the propagation of weak shock waves into an acoustic shadow zone. Although the present study is carried out at the laboratory scale, the initial motivation is related to the propagation of a sonic boom in the atmosphere. With the recent development of low-boom aircraft concepts, the public acceptability of overland supersonic flight and of sonic boom exposure is still under study [1–4]. When a sonic boom propagates in a downward-refracting atmosphere, the ground area directly reached by acoustic rays is called the sonic boom primary carpet. The ray paths tangent to the ground define the lateral cutoff between an illuminated and a shadow zone and thus define the extent of the primary carpet [5]. A secondary carpet, with smaller overpressure levels, may also result from refraction in the upper atmosphere. As ray paths are randomly modified by turbulence, the boom carpets may be randomly extended or reduced, modifying the carpet width where the boom is heard [6–8]. The ground elevation profile may also create shadow zones [9,10]. The atmospheric turbulence is expected to have an influence on wave propagation and then on the sound level. The aim of the present paper is to highlight the effects of turbulence on the propagation of weak shocks into a shadow zone. In particular, the question of whether turbulence would lead or not to an extension of the primary carpet is examined.

Without turbulence, analytical expressions for the diffracted sound field into the shadow zones [5,11] show a good agreement compared to Concorde ground signatures [5], to outdoor measurements [12,13], and also to laboratory experiments [14–16]. With turbulence, a statistical analysis of the random distortion of aircraft signatures has been conducted to evaluate the influence of atmospheric turbulence [17]. It was found that atmospheric turbulence is responsible for the random characteristics of sonic boom signatures [1,18–21].

However, during field measurements of sonic boom signatures, the atmospheric conditions cannot be sufficiently characterized. The separation between different effects, such as ground reflections, propagation through turbulence, or refraction, is therefore not possible. These reasons have motivated the development of alternative methods to outdoor measurements. Realistic numerical simulations of sonic boom propagation and focusing in a homogeneous atmosphere were performed over the last decades [22,23]. The propagation into shadow zones, generated from refraction or topography, was later examined [9,24]. The random scattering caused by the atmospheric turbulence was also studied for the simple case of monochromatic waves [25] or for more realistic sonic boom waveforms [26–31]. The combined effects of nonlinear propagation, scattering by turbulence, and propagation into a shadow zone were also studied recently [32]. However, the computational cost of long-range nonlinear propagation of shockwaves through turbulence in a refracting atmosphere still limits the statistical analysis. Another approach is to perform well-controlled laboratory-scale experiments in which the different effects are studied separately. Acoustic propagation in a refracting medium has been studied at the laboratory scale [16,33] in an enclosure with a sound-speed gradient. Laboratory-scale experiments may also take advantage of the analogy between the propagation over flat ground in a refracting atmosphere and the propagation over a convex surface in a homogeneous atmosphere [14,34,35]. This analogy is valid for constant sound-speed gradients over a rigid ground if all geometrical quantities (source height, propagation distance into the shadow zone, wavelength) are small compared to the radius of curvature. Using this analogy, the propagation into an acoustical shadow zone with turbulence has been experimentally studied by Wasier [36]. This experiment highlighted the effects of wave scattering due to turbulence into the shadow zone. The combined effects of nonlinear propagation through a turbulent atmosphere were studied later [37–41]. At the laboratory scale, spark sources are used to produce weak shocks in air whose characteristics are now well understood [42–46]. These studies showed that turbulence causes *N*-wave distortion. Regarding the combined effects of *N*-wave propagation, turbulence, and shadow zone, an increase of the pressure level is expected on average in the shadow zone. However, the random effects of turbulence are not well described in the literature; a statistical analysis is therefore desirable.

In the present work, a controlled experiment is performed at the laboratory scale, with *N*-waves obtained using an electrical spark source. Thermal turbulence is generated using a heating grid of electrical resistors. Building upon a previous study by the present

Presented as Paper 2024-3186 at the 30th AIAA/CEAS Aeroacoustics Conference, Rome, June 4–7, 2024; received 28 October 2024; accepted for publication 27 April 2025; published online 3 June 2025.

*edouard.salze@ec-lyon.fr (Corresponding Author).
†CNRS, Ecole Centrale de Lyon, INSA Lyon.
‡Member AIAA.

authors [41], a curved surface has been added to create an acoustic shadow zone. The geometrical scaling is about 1:1000 for the source wavelength, the propagation distance, and the turbulence outer scale, relevant for sonic boom propagation in a refracting atmosphere [47].

However, compared to real sonic boom signatures [48], the spark source exhibits a higher frequency content and a higher pressure level. This leads to an overestimation of absorption and nonlinear effects. The turbulence intensity may also be higher in the present down-scaled experiment. While this controlled laboratory experiment does not exactly model the propagation of sonic boom at scale, it highlights the effects of the shadow zone and turbulence, either separately or combined.

The rest of the paper is organized as follows: The experimental setup is detailed in Sec. II. Results are given and discussed in Sec. III. The analytical expression used in the present paper in Sec. III.A.1 is indicated in the Appendix.

II. Experimental Setup

The experimental setup is outlined in Fig. 1. Measurements were conducted in the anechoic chamber of the Centre Acoustique at École Centrale de Lyon, France. A curved boundary, made of a 5-mm-thick polyvinyl chloride plate, is used to simulate an upward-refracting atmosphere as in Berry and Daigle [14]. The plate was twisted to form a cylinder of radius $R = 1.14$ m, which corresponds to a sound-speed gradient of approximately $c_0/R = 298\ \text{s}^{-1}$. Short-duration and high-pressure spherical waves are generated using an electrical spark source, noted S in Fig. 1. The spark source is made of two tungsten electrodes separated by an air gap of 20 mm, driven by a high-voltage supply of up to 20 kV. Once the potential breakdown of the air is reached, a spark is formed and a pressure pulse is generated. Because of nonlinear propagation, the pressure pulse turns into a shockwave a few centimeters away from the electrodes [46].

Pressure waves are recorded using an 1/8 in. condenser microphone (Brüel & Kjær type 4138), flush-mounted without its protection grid into a plane baffle to limit diffraction on the edges of the microphone. Microphone conditioning is performed using a modified Brüel & Kjær type 2690 conditioner, whose frequency bandwidth has been extended up to 200 kHz, beyond the microphone frequency cutoff. Signals are recorded over 12 bits at a sampling frequency of 10 MHz using a National Instruments type 5105 device. The propagation distance and microphone angle of incidence are remotely controlled using a motorized device.

In this paper, interest is focused on the front shock peak pressure and on the rise time, $P_{\max}$ and τ, respectively. The rise time is defined as the time interval needed for the pressure to rise from 10 to 90% of the peak pressure $P_{\max}$. Without turbulence, a pressure level of 1170 Pa is measured at a distance $r = 250$ mm from the electrodes [41]. Because of spherical spreading, linear absorption, and nonlinear effects, the pressure level decreases with the distance.

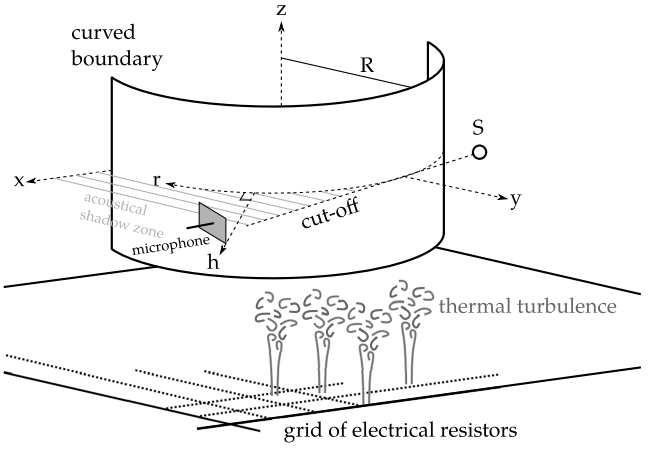

Fig. 1 Schematic of the experimental setup (not to scale).

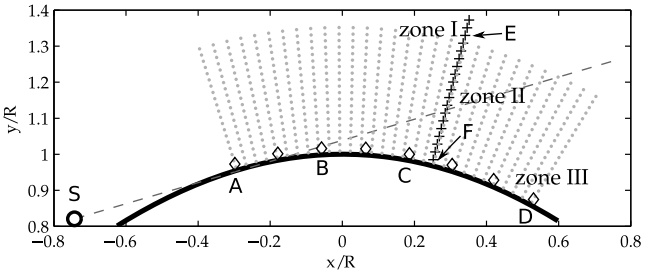

Fig. 2 Microphone positions for the different measurement series (see also Table 2): ◦, map-*nt*; +, *h*-wt; ◇, *r*-nt and *r*-wt. ○: position of the source S; ——: curved boundary; – – –: limiting ray between the illuminated zone and the shadow zone when diffraction is not considered.

Using optical methods, it has been shown that the pressure rise time is less than 1 μs at a distance of 1 m from the source [45,46]. However, acoustical measurements of such steep pressure rises are not possible due to the limited bandwidth of commercially available microphones. In this study, the microphone bandwidth is limited to 140 kHz, and thus a rise time estimation of the order of 3 μs would correspond to the rise time of the microphone and not of the pressure wave [41,44,46]. The resonance of the microphone also generates oscillations on the measured waveforms (see Fig. 3 and the Appendix of [41]). Despite these limitations, the rise time is discussed in the present paper since a significant increase in the rise time is observed in the shadow zone.

Thermal turbulence is generated through Joule heating using a grid of electrical resistors. The overall size of the grid is 4.4 m × 1.1 m, dissipating a total of 64 kW of electrical power. The resistors are arranged with a 9-cm-square mesh. This dimension was chosen so that the turbulence length scale matches the atmospheric length scale at the laboratory scale. Fully developed turbulence is obtained 160 cm above the grid by natural mixing of thermal plumes. The field of thermal turbulence has been characterized using constant current temperature probes and a thermocouple. Away from the boundary, a mean temperature of 308 K and root mean square temperature fluctuations of 5 K are measured. The corresponding sound speed standard deviation is about 0.8% [41]. The turbulent temperature fluctuations can be described with excellent agreement by a modified von Kármán model [36, 41,49]. The ability to model the turbulent spectrum is important because, once the model is known, it can be easily synthesized for numerical simulations [50,51].

The different positions reached by the measuring microphone are detailed hereafter, where "nt" stands for "no turbulence," and "wt" for "with turbulence": a series in the (x, y) plane without turbulence, named **map-nt**; a series without turbulence, h being varied, named ***h*-nt**; a series with turbulence, h being varied, named ***h*-wt**; a series without turbulence, r being varied, named ***r*-nt**; and a series with turbulence, r being varied, named ***r*-wt**. The source position ($x/R = 0.74$, $y/R = 0.82$) is not varied in this paper. The different measurement series are sketched in Fig. 2 and also detailed in Table 1. Without turbulence, 60 spark shots have been recorded. With turbulence, because of a larger variability, this number is increased up to 500 or 2000, depending on the measurement series (see Table 1). Six microphone positions named A to F are also considered in the following sections (see Table 2).

Table 1 Definition of the measurement series (see also Fig. 2)

Series	Shots	Positions	min (h/R)	max (h/R)	min (r/R)	max (r/R)
map-nt	60	600	0.02	0.37	0.47	1.32
h-nt	60	48	0.02	0.42	0.90	0.90
h-wt	500	19	0.02	0.42	0.90	0.90
r-nt	60	8	0.02	0.02	0.47	1.32
r-wt	2000	8	0.02	0.02	0.47	1.32

Table 2 Coordinates of the microphone positions from A to F (see also Fig. 2)

Position	x/R	y/R	r/R	h/R
A	−0.30	0.97	0.47	0.02
B	−0.06	1.02	0.71	0.02
C	0.19	1.00	0.96	0.02
D	0.53	0.87	1.32	0.02
E	0.34	1.33	0.90	0.37
F	0.25	0.98	0.90	0.02

III. Results and Discussion

A. Pressure Waveforms

1. Without Turbulence

Without turbulence, examples of waveforms are plotted in Fig. 3. In the illuminated zone, at position E (see Fig. 2), the average pressure level is ∼150 Pa and the rise time is ∼2.6 μs on average. At this distance from the source, the pressure level is in good agreement with previous studies [41,43]. Without turbulence, the peak pressure standard deviation is about 2% because of random variations of the spark shape over the 2 cm air gap between the electrodes. The waveforms in the illuminated region exhibit well-known features with two shocks. The oscillations observed on the waveforms are due to the microphone resonance around 140 kHz [41]. A reflected wave can also be identified as a small peak around $t = 4$ ms.

In the acoustical shadow zone at position F (see Fig. 2), the pressure waveforms exhibit different features. The waveform is less symmetrical: the negative peak pressure is lower than the positive peak pressure in absolute value. The positive peak pressure is 25 Pa, and the rise time is 17 μs. At the same distance from the source, without a curved boundary, the pressure level would be around 200 Pa [41] and the pressure rise time of the order of 1 μs [45].

A comparison of the pressure waveforms measured along the curved surface with the ones computed from the analytical solution from Coulouvrat [5] is proposed in Fig. 4. The analytical expression is indicated in the Appendix. The analytical waveforms have been computed for a fixed height h, increasing the distance r/R from 0.47 to 1.32 (see Table 1). The curved boundary is supposed to be perfectly rigid, i.e., $q(\omega) = 0$. An ideal N-wave model is used for the incident pressure waveform p_0. The incident waveform characteristics are set equal to the ones measured without the curved boundary at the same distance from the source [41]. A good agreement is obtained between the measured and the analytical waveforms (see Fig. 4). In particular,

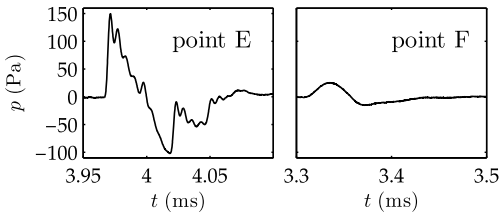

Fig. 3 Typical measured waveforms without turbulence (h-nt series). Left: point E, illuminated zone, $x/R = 0.34$, $y/R = 1.33$. Right: point F, shadow zone, $x/R = 0.25$, $y/R = 0.98$.

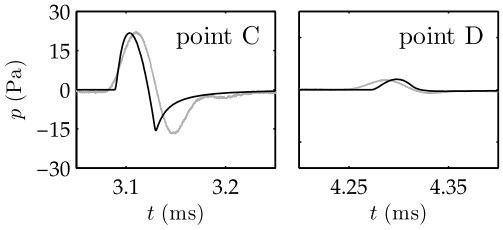

Fig. 4 Comparison between the analytical expression (see Appendix) and the measured waveforms without turbulence (r-nt series): Left: point C, $x/R = 0.19$, $y/R = 1.00$. Right: point D, $x/R = 0.53$, $y/R = 0.87$.

the peak pressure is correctly predicted within less than 5%. This result is interesting because it proves that the linear analytical expression is valid for an incident N-wave. This indicates that the propagation into the shadow zone occurs because of linear diffraction mechanisms, which are well described by the analytical expression, even for short propagation distances into the shadow zone.

2. With Turbulence

Four examples of waveforms measured with turbulence (in the shadow zone, position D) are plotted in Fig. 5. Note that the pressure level p has been normalized by the reference pressure P_{ref}, measured without turbulence at the same location. First, the systematic delay between the reference waveform and the ones measured with turbulence is due to the increase in mean temperature caused by the heating. As was observed without the curved boundary [41], additional random fluctuations of the time of arrival are due to different propagation paths between those four examples. With turbulence, because of the random propagation medium, strongly distorted waveforms are observed: waveforms with a high amplitude, amplified by a factor of up to 8, and with a sharp front shock (see Fig. 5a); waveforms similar to the ones measured without turbulence (see Fig. 5b); waveforms with a very large rise time of up to 20 μs (see Fig. 5c); and waveforms with multiple peaks and a plateau (see Fig. 5d). These wave profiles are very similar to the ones measured without a reflecting boundary [37,41]. These waveforms also present strong similarities to sonic boom profiles measured in the atmosphere [17,20,52]. In a free field, compared to the case without turbulence, amplification factors of up to 3 were observed [41], resulting from random focusing or attenuation. Inside an acoustic shadow zone, peak pressure amplifications of up to 8 are likely due to scattering from the illuminated region into the shadow zone rather than random focusing or attenuation.

The corresponding spectra amplitudes are plotted in Fig. 6, where the reference spectrum without turbulence is in gray, and the spectrum with turbulence is in black. The level 0 dB is the maximum of the reference spectrum, obtained without turbulence. The reference spectrum exhibits a main lobe between 100 Hz and 20 kHz. Note that the level of –50 dB observed above 20 kHz corresponds to the noise level of the acquisition system. An example of a high-amplitude waveform, amplified by a factor of 7, is plotted in Figs. 5a and 6a. Compared to the reference waveform, an amplification of more than 40 dB is found above 20 kHz. Between 20 and 140 kHz, a series of lobes is visible. These lobes are related to the finite length of the pressure waveform. The microphone high-frequency cutoff is clearly visible above 140 kHz. It is therefore possible that the pressure might have been amplified well over the microphone cutoff frequency. The three other examples (see Figs. 6b–6d) differ from

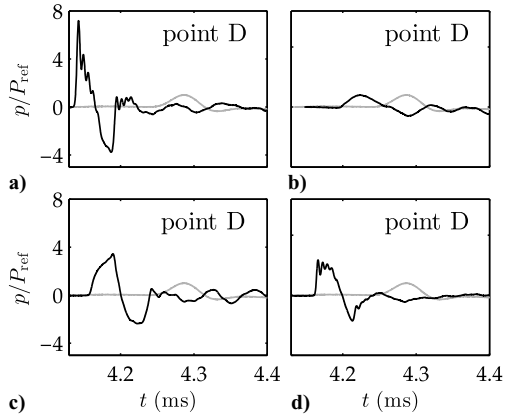

Fig. 5 Examples of waveforms measured at point D ($x/R = 0.53$ and $y/R = 0.87$) with turbulence, normalized by the reference peak pressure without turbulence. ——: examples of waveforms with turbulence (r-wt series). ——: reference waveform at the same position without turbulence (r-nt series). a) High amplitude, b) low amplitude, c) large rise time, and d) waveform with multiple peaks and a plateau.

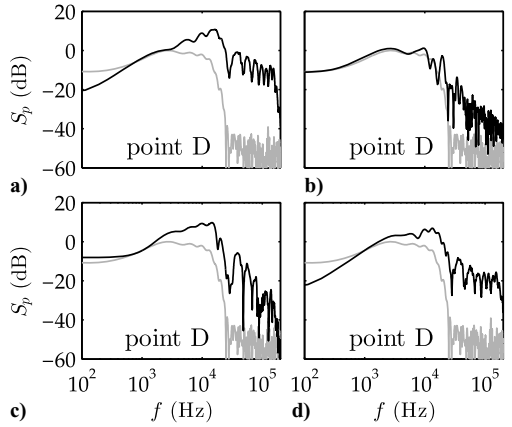

Fig. 6 Pressure spectra S_p of the waveforms from Fig 5, all measured at point D ($x/R = 0.53$ and $y/R = 0.87$), normalized by the maximum of the reference spectrum without turbulence.

the reference spectrum by an amplification in the high-frequency domain. The noticeable aspect is that turbulence would always amplify the pressure level in the range from 2 to 140 kHz, which was not the case in the illuminated region [41].

B. Peak Pressure

Without turbulence, a first overview of the peak pressure is represented as a pressure map in the (x, y) plane (see Fig. 7). This figure has been obtained from 600 measurement points defined in Fig. 2, homogeneously distributed between $r/R = 0.47$ and $r/R = 1.32$, and between $h/R = 0.02$ and $h/R = 0.37$ (see Table 1). In the illuminated zone, pressure levels of up to 350 Pa are measured (see Fig. 7). In the shadow zone, the pressure level vanishes as the wave propagates deep into the shadow zone. Considering the noise impact of supersonic aircraft, the atmospheric conditions and the existence of shadow regions are therefore likely to be of major importance. In the presence of a negative sound-speed gradient, the ground area of maximum annoyance is fixed by the positions of shadow zones.

The peak pressure is plotted in Fig. 8 as a function of h (left figure) and r (right figure). In the present experiment, the shadow zone is reached if $h/R < 0.2$. In Fig. 8, mean values of the peak pressure are indicated as black dots (without turbulence) and black crosses (with turbulence). In addition, the dark gray area and the light gray area contain all values of the peak pressure, without and with turbulence, respectively. Measurements without the curved boundary are also reproduced from a previously published experiment [41]. In the next sections, the peak pressure is analyzed in three zones, named I, II, and III (see Fig. 2).

1. *Zone I: Illuminated Zone*

Zone I is the region in the illuminated zone where the time delay between the direct wave and the reflected wave is sufficient to avoid interference (here if $h/R > 0.3$, see Fig. 2 at left, or if $r/R < 0.6$ in Fig. 2 at right). In this zone, without turbulence, when h is reduced, P_{ref} increases because of the reduced distance of propagation. Measurements of the reference pressure P_{ref} without turbulence are in very good agreement with spark-generated N-wave measurements in a free field [43], within less than 2% fluctuation. This is also in good agreement with previously published data [32,41]. With turbulence, the mean peak pressure obtained from 500 spark shots is equal to 0.87 times the reference value measured without turbulence (see Fig. 8 at left). This is also consistent with measurements without the curved boundary [41]. As was discussed before by other authors [30,37,39], this attenuation of the peak pressure is associated with a random variability of the pressure. At an altitude of $h/R = 0.4$, the peak pressure can reach values between 0.34 and

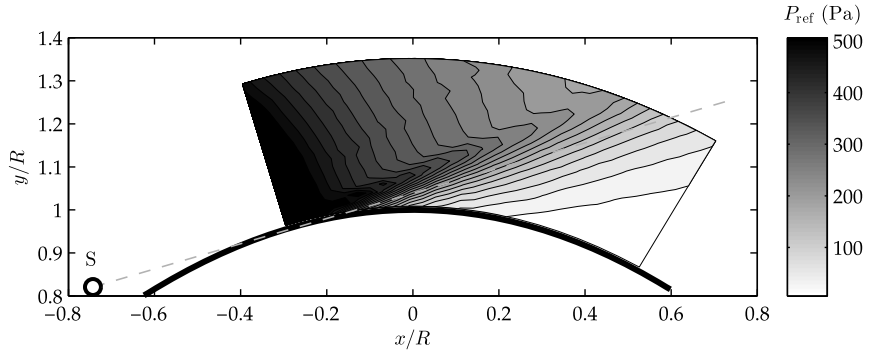

Fig. 7 Contours of the reference peak pressure P_{ref} without turbulence, from 600 measurement points distributed in the (x, y) plane (map-nt series).

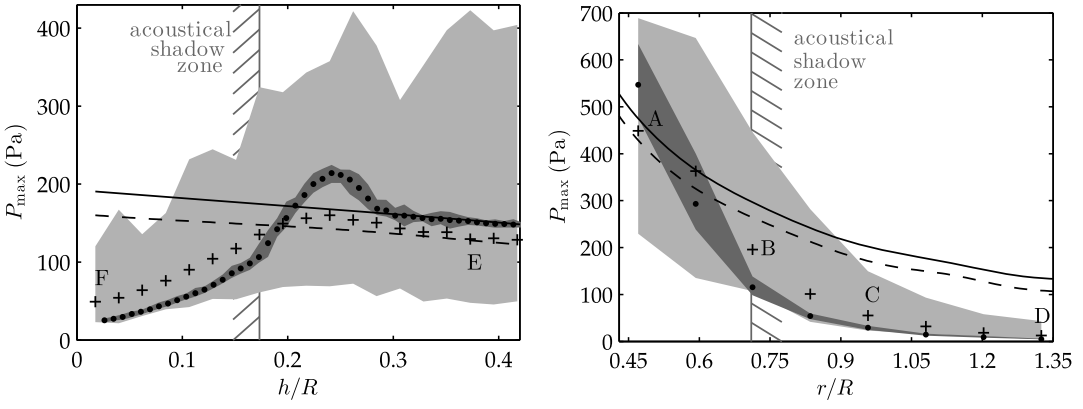

Fig. 8 Positive peak pressure $P_{\max}$. ·: reference peak pressure P_{ref} measured without turbulence (h-nt series); +: mean value $\langle P_{\max} \rangle$ with turbulence (h-wt series), ——: measurements from [41], without the curved boundary and without turbulence; - - - : measurements from [41], without the curved boundary and with turbulence. ■: area containing all measurements without turbulence (60 shots per position); ■: area containing all measurements with turbulence (500 shots per position). Left: as a function of height h. Right: as a function of propagation distance r into the shadow zone.

2.75 times the reference value without turbulence. It means that far away from the curved boundary, the peak pressure can be randomly attenuated or amplified by a factor of up to 3 approximately, as is the case without the curved boundary [41].

2. *Zone II: Close to the Limiting Ray*

Zone II is the region close to the limiting ray between the illuminated and the shadow zones (see Fig. 2), sometimes called the *penumbra* region. Without turbulence, around the limiting ray, in the penumbra region, the peak level is lower than in a free field, but just above the limiting ray, an amplification of the peak pressure level is observed. The maximum amplification, by a factor of about 1.4, is located at $h/R = 0.24$. This phenomenon, which is due to diffraction and reflection from the curved boundary, has already been documented in the literature [5]. With turbulence, an amplification is still visible, but on average the amplification is lower. However, an amplification by a factor of 1.4 would occur for every single wave propagating through turbulence. Indeed, the different propagation paths from one spark shot to another lead to different times of arrival. The maximum amplification then occurs at different altitudes from one wave to another; a lower amplification is therefore observed on average at a given position. In this region close to the limiting ray, the peak pressure level varies between 0.43 and 2.25 times the reference value without turbulence (see Fig. 8).

3. *Zone III: Shadow Zone*

Zone III is the shadow zone where the reference pressure level without turbulence rapidly vanishes (see Fig. 2). For instance, close to the surface ($h/R = 0.02$), the mean peak pressure is 25 Pa without turbulence. Compared to free-field measurements, an attenuation by a factor of more than 7 is observed for similar propagation distances. In the shadow zone, thermal turbulence causes an amplification of the mean peak pressure. On average, the peak pressure is amplified by a factor of 2 at $h/R = 0.02$. As h is decreased, strong fluctuations of the peak pressure occur with turbulence, as is the case outside the shadow zone. With turbulence, the lowest peak pressures correspond to the reference value measured without turbulence (see Fig. 8), while the highest peaks can be up to eight times the reference value deep into the shadow zone. This result is remarkable for two reasons. First, it shows that huge pressure fluctuations still exist deep in the shadow zone, whereas one would expect small fluctuations if the main propagation mechanism in the shadow is diffraction on the curved surface, where sound speed inhomogeneities decrease to zero. Second, turbulence does not attenuate the pressure in the shadow zone. On the contrary, it is observed that, as h decreases, the peak pressure is always larger than the reference value measured without turbulence. Those two observations confirm that the dominant effect of turbulence is to diffuse waves from the illuminated zone into the shadow zone.

The question now is whether turbulence would cause an expansion of the illuminated area at the ground. A criterion can be based on the detection at the ground in the geometric shadow zone of higher pressure peaks with turbulence than the limit value detected without turbulence at the cutoff position between the illuminated and shadow zones. This criterion can be applied for each ground position by considering either the average value of the pressure peaks or the wave of greatest amplitude observed at that point. Without turbulence, a maximum pressure of about 115 Pa is measured at the cutoff at $r/R = 0.71$ (see Fig. 8, right figure). With turbulence, this value of 115 Pa is reached on average at $r/R = 0.81$, and values higher than 115 Pa can be observed up to $r/R = 1.03$. Thus, for the present experiment, it can be concluded that the illuminated zone has therefore been extended from $r/R = 0.71$ up to 0.81 on average, and that values as high as in the illuminated areas are observed up to $r/R = 1.03$. Similar effects are expected for the sonic boom: the lateral cutoff should be modified by turbulence, and the width of the primary carpet should increase. Of course, the extension by turbulence effects of the ground area where the sonic boom could be annoying will depend on the one hand on the turbulence (intensity and spectrum) and on the other hand on the shadow zones created by sound-speed gradients and/or by the ground elevation profile in the direction of wave propagation.

C. Peak Pressure Probability Distributions

In this section, peak pressure statistics are analyzed in detail from the two datasets h-wt and r-wt (see Table 1). The consistency from one spark to another of wave duration, peak pressure, and other parameters was previously checked [40,41,44,53]. Therefore, the properties of the incident waves are assumed to be identical from one spark to another. The statistics of the first data set with turbulence (h-wt series) have been computed over 500 spark shots per microphone position. The second set of statistics (from the r-wt series) has been computed over 2000 spark shots per microphone position.

1. *Density of Probability W*

The density of probability W_ν of the variable ν is defined from the probability Pr for ν to belong to a certain interval $\mathcal{A}$ as

$$Pr[\nu \in \mathcal{A}] = \int_{\mathcal{A}} W_\nu \, \mathrm{d}\nu$$

It is convenient to perform the statistical analysis by normalizing the peak pressure by its average value; the variable $P^* = P_{\max}/\langle P_{\max}\rangle$ is therefore considered. The measured probability density W_{P^*} is plotted as histograms in Fig. 9 for positions A, B, C, and D (see Fig. 2).

At position A, the peak pressure distribution is nearly symmetrical (see Fig. 9a) and centered around the mean value $P^* = 1$. When the propagation distance is increased (up to position D), waveforms with a high pressure level are observed (see Fig. 5a). The statistical distribution is less symmetrical, and a tail is formed at high amplitudes up to $P^* = 2$ (see Figs. 9b–9d). A similar behavior has been previously detailed in the case of linear harmonic waves for increasing propagation distances [49], in the case of N-waves propagating through kinematic turbulence for increasing turbulence intensity [37], and in the case of high-amplitude N-waves propagating through thermal turbulence for increasing propagation distances [41]. Compared to previously published statistical distributions without boundary [41] for similar propagation distances, the statistical distribution in a shadow zone exhibits a shorter tail (see Fig. 9d). For instance, values of P^* up to 3 were measured with no boundary [41], whereas it is not the case in the shadow zone. This might indicate that the tail distribution is formed during the propagation in the illuminated zone.

Following previous works [37,41,49], it is appropriate to describe the peak pressure probability densities using generalized Gamma distributions, defined as

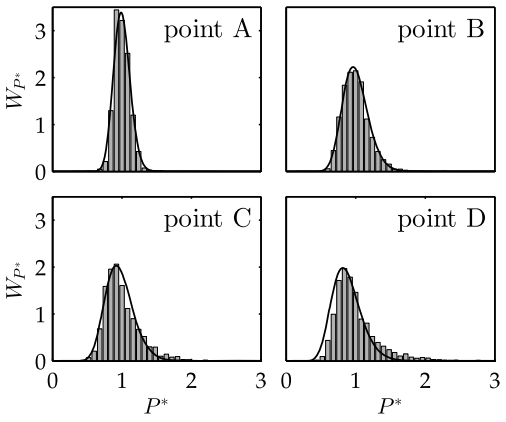

Fig. 9 Probability density W_{P^*} of the normalized positive peak pressure $P^* = P_{\max}/\langle P_{\max}\rangle$ for four positions: point A ($x/R = -0.30$ and $y/R = 0.97$), point B ($x/R = -0.06$ and $y/R = 1.02$), point C ($x/R = 0.19$ and $y/R = 1.00$), and point D ($x/R = 0.53$ and $y/R = 0.87$). Bar graph: measured values, ——: Generalized gamma distribution.

$$W_{P^*} = \frac{bd^a}{\Gamma(a)} P^{*ab-1} \exp(-dP^{*b})$$

where Γ is the gamma function, and a, b, and d are parameters depending upon the turbulence intensity and/or upon the propagation distance. These parameters have been estimated from the experimental statistical distributions (see Fig. 9) using the second and third statistical moments of the statistical distributions, respectively, denoted m_2 and m_3:

$$m_2 = \int_0^{+\infty} P^{*2} W_{P^*} \mathrm{d}P^* = \frac{\Gamma(a)\Gamma(a+2/b)}{\Gamma^2(a+1/b)}$$

and

$$m_3 = \int_0^{+\infty} P^{*3} W_{P^*} \mathrm{d}P^* = \frac{\Gamma^2(a)\Gamma(a+3/b)}{\Gamma^3(a+1/b)}$$

The resulting values of a and b are plotted in Fig. 10 as a function of r for a fixed h, and in Fig. 11 as a function of h for a fixed r. White symbols stand for measurements as a function of h. Black symbols represent measurements as a function of r. White symbols containing a cross indicate free-field measurements of a previous study [41] for the same propagation distance. In the previously defined zone I (illuminated zone when $h/R > 0.3$, see Fig. 2), an excellent agreement is found with the previously published free-field measurements (indicated as a cross in Fig. 11), within 1% for coefficient a, and within 10% for coefficient b. In the shadow zone, the measurements as a function of h (indicated as a black filled square in Fig. 11) are in good agreement with those performed as a function of r. The corresponding modeled probability densities W_{P^*} are plotted in Fig. 9. Good agreement is found between the experimental distributions and the empirical model. Once the coefficients a and b are known from a limited number of measurements, a practical advantage of this method is that an estimation of the probability densities can be made in regions where measurements have not been performed.

2. *Cumulative Probability w*

In order to analyze the occurrence of amplified waveforms in the shadow zone, the cumulative probability has been computed. To highlight the peak pressure amplification due to turbulence, it is convenient to use the variable $P_{\max}/P_{\mathrm{ref}}$ (different from P^*). The

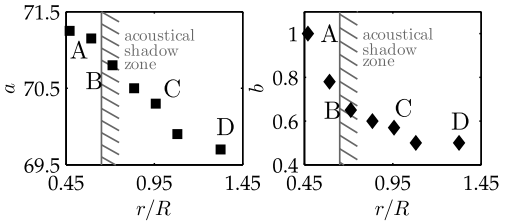

Fig. 10 Coefficients a (at left) and b (at right), as functions of r/R (r-wt series). ■: coefficient a, ◆: coefficient b.

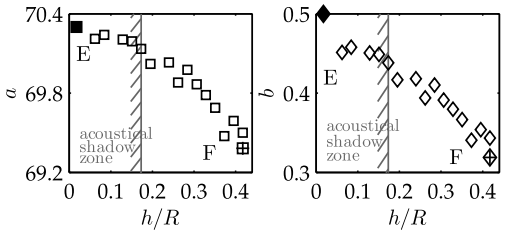

Fig. 11 Coefficients a (at left) and b (at right), as functions of h/R. □, ◇: coefficients a and b from h-wt series. ■, ◆: coefficients a and b from r-wt series close to the boundary ($x/R = 0.30$, $y/R = 0.97$). +: coefficients a and b from a previous study without the curved boundary [41].

Table 3 Probability $w(\alpha)$ for the peak pressure $P_{\max}$ to be amplified by a factor 1, 2, 4, or 8, because of turbulence, as a function of propagation distance into the shadow zone

r/R	$w(1)$, %	$w(2)$, %	$w(4)$, %	$w(8)$, %
0.59	87.00	0.15	0	0
0.71	99.65	10.75	0	0
0.83	99.00	30.90	0.10	0
0.96	98.50	30.05	0.25	0
1.08	99.55	52.10	1.70	0
1.32	99.85	66.05	4.95	0.05

cumulative probability $w(\alpha)$ is defined as the probability that $P_{\max}/P_{\mathrm{ref}}$ exceeds some threshold α as

$$w(\alpha) = \int_{\alpha}^{+\infty} W_{P_{\max}/P_{\mathrm{ref}}} \mathrm{d}(P_{\max}/P_{\mathrm{ref}})$$

Results obtained using this definition are given in Table 3 for increasing propagation distance r, with $h/R = 0.02$.

The probability $w(1)$, of observing inside the shadow zone a wave whose amplitude is greater with turbulence, is of 87% for the first measurement point in the shadow zone ($r/R = 0.59$). This probability reaches values close to 100% as the propagation distance r is increased. The probability $w(2)$, of observing a peak pressure doubling at the first point of the shadow zone, is almost zero, and then it increases continuously up to 66% for $r/R = 1.32$. In a similar way, the probability $w(4)$, of having a peak pressures amplification by a factor of 4 or more, is smaller than 1% if $r/R < 1.08$. This probability $w(4)$ increases with the distance r to reach a value of 5% at $r/R = 1.32$. At last, the probability $w(8)$, of observing with turbulence a peak pressure amplification by a factor of 8, is null, except for the longest distance $r/R = 1.32$, where it is about 0.05%. Note that this value of 0.05% corresponds to a single wave registered over a number of 2000 registered waveforms for this distance r. Compared to measurements without boundary, the cumulative probability w from Table 3 exhibits noticeable differences. During the free-field propagation through thermal turbulence, random attenuation or focusing has been observed, and the probability $w(1)$ was found of the order of 20% [41]. It is not the case in the present experiment, where $w(1)$ is nearly 100% deep into the shadow zone. In a free field, a peak pressure doubling because of turbulence is a rare event, with no more than 0.6% probability [41]. On the contrary, a peak pressure doubling in the shadow zone is a common event, with a probability on the order of 66%. Peak pressure amplifications up to 8 times are also observed.

D. Rise Time

In this section, interest is focused on the pressure rise time τ, defined as the time interval between 10 and 90% of the positive peak pressure. In real atmospheric conditions, it has been reported [54,55] that the atmospheric turbulence causes an increase in sonic boom rise times, on average. This effect has also been observed in laboratory-scale experiments [39,40] or using numerical modeling [30]. In the context of laboratory-scale experiments, rise time analysis must be performed carefully because of the limited bandwidth of commercially available microphones. For example, 1/8 in. condenser microphones do not allow the measurement of rise times smaller than 2.6 μs. It is known from optical measurements that the actual rise time is less than 1 μs at a distance of 1 m away from the source [45]. Therefore, measurements of the order of 3 μs are likely to be the rise times of the microphone. Discussions about the smallest rise time values are therefore meaningless. However, a large increase in the rise time is observed during the propagation through turbulence [41] or during the propagation into an acoustical shadow zone. In the absence of suitable high-frequency wideband sensors, only large values of the rise time are discussed in the following.

In Fig. 12, the average rise time $\langle\tau\rangle$ and the extreme values are plotted as functions of h for a fixed $r/R = 0.90$, with and without turbulence. In the illuminated zone ($h/R > 0.2$), a value

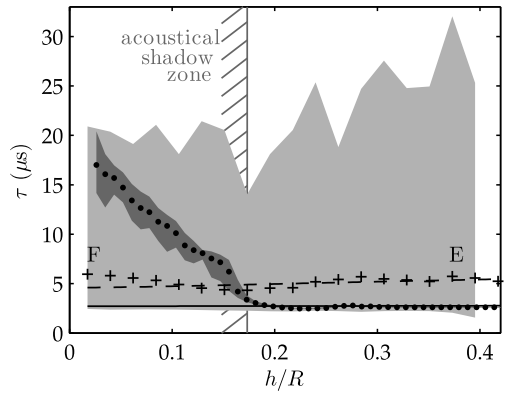

Fig. 12 Front shock rise time τ as a function of height h. ·: reference rise time $\langle\tau_{\text{ref}}\rangle$ measured without turbulence (h-nt series). +: mean value $\langle\tau\rangle$ with turbulence (h-wt series). ——: measurements from a previous study [41], without the curved boundary without turbulence. - - -: measurements from a previous study [41], without the curved boundary with turbulence. ■: area containing all measurements without turbulence. ■: area containing all measurements with turbulence.

of $\langle\tau\rangle = 2.7$ μs is obtained without turbulence, which is the rise time of the microphone and not of the pressure. With turbulence, its mean value increases up to $\langle\tau\rangle = 5$ μs. The smallest measured value is $\tau = 2.6$ μs, whereas the longest rise time is $\tau = 31$ μs. These values are consistent with previously published measurements without the curved boundary [41].

In the shadow zone ($h/R < 0.2$), on average, a large increase in the rise time is observed without turbulence, compared to free-field measurements. For example, at the smallest altitude $h/R = 0.02$, the rise time is $\tau = 17$ μs on average. As observed in Sec. III.A, propagation in the shadow zone attenuates high frequencies, which results in increased rise times. This increase of the rise time has been used by other authors [12,13] during outdoor experiments as a criterion for determining the location of the shadow zone. With turbulence, it is found that the mean rise time is nearly constant in the shadow zone, around 6 μs. Values between 3 μs and 21 μs are measured (see also Fig. 5c). As was detailed in a previously reported experiment [41], rise times that are multiples of the microphone rise time are observed with a higher probability because of the oscillations caused on the waveforms by the microphone's resonance frequency. It is also the case in the present experiment.

IV. Conclusions

Propagation into a shadow zone of initially high-amplitude N-waves has been studied at the laboratory scale in the presence of thermal turbulence. The effects purely related to the shadow zone and those purely related to the propagation through turbulence have been identified. The waveform, the peak pressure, and the rise time of the pressure waves were analyzed. For this purpose, a large number of waveforms were recorded after propagation in the shadow zone, without or with turbulence.

Measurements in the illuminated region exhibit an excellent agreement with previously published free-field measurements at the laboratory scale, without or with turbulence. Without turbulence, pressure waveforms recorded in the shadow zone are found in good agreement with the linear analytical solution. This indicates that, even for initially high-amplitude N-waves, sound propagates into the shadow zone through linear diffraction mechanisms. Into the acoustical shadow zone, the pressure level rapidly vanishes to a few pascals. Considering the noise impact of supersonic aircraft, the ground area of maximum exposure is therefore determined by the position of shadow zones. With turbulence, peak pressure statistics were computed and described using a generalized gamma empirical model as a function of height for a fixed propagation distance or as a function of distance for a fixed altitude. During previously free field measurements at the laboratory scale, a random attenuation or a random focusing has been observed. It is not the case in the shadow zone, where a systematic amplification of the peak pressure is observed. A doubling of peak pressure is a common event, and the amplification can be much higher, up to a factor of 8. In the presence of turbulence, the pressure level in the shadow zone is dominated by pressure waves previously scattered by turbulence from the illuminated region into the shadow zone. Transferring these results to the sonic boom is not straightforward, but when the atmospheric turbulence is significant, one can expect a widening of the sonic boom primary carpet.

Appendix: Analytical Expression into the Shadow Zone

Without turbulence, creeping-wave theory predicts that sound propagates into the shadow zone by successive diffractions on the ground [11]. Under the assumption of linear acoustics, analytical expressions for the diffracted sound field into the shadow zone have been reported [11,14,16], provided that the refracted rays can be approximated as circles of radius R. If the altitude y remains small compared to R, the assumption of circular refracted rays is valid for a linear profile of sound celerity [16] $c(y) = c_0(1 - (y/R))$, for the so-called "bilinear" profile [14] $c(y) = c_0/(\sqrt{1 + 2y/R})$, and for the exponential profile $c(y) = c_0 \exp^{-y/R}$, where $c(y)$ is the vertical sound-speed profile and $c_0 = c(y = 0)$. The acoustic pressure in the acoustic shadow zone can be expressed as [5]

$$p(t) = \mathcal{F}\left[\mathcal{F}^{-1}[p_0(t)] \sum_{n=1}^{N} e^{ik_n r^\star} \frac{A_i(b_n - (h/l)e^{2i\pi/3})}{A_i'(b_n)^2 - b_n A_i(b_n)^2}\right] \quad \text{(A1)}$$

where $N \to \infty$ is the number of modes, $\mathcal{F}[.]$ denotes the Fourier transform of a given signal, p is the acoustic pressure in the shadow zone, p_0 is the incident pressure at the cutoff, $r^\star$ is the propagation distance in the shadow zone, h is the altitude, A_i is the Airy function, and A_i' its derivative. The parameter $l = (R/2k_0^2)^{1/3}$ is a measure of the diffraction thickness, and k_0 is the acoustic wavenumber. The terms b_n are the roots of the following equation:

$$A_i'(b_n) + q(\omega)A_i(b_n)e^{2i\pi/3} = 0 \quad \text{(A2)}$$

where $q(\omega) = ik_0 Y_s l$ represents the effect of ground impedance, with Y_s being the ground admittance. For a rigid ground, $q = 0$, and the terms b_n are simply the roots of the derivative A_i' of the Airy function. At last, the wavenumbers k_n are expressed as

$$k_n = k_0\left(1 + \frac{1}{2}e^{-2i\pi/3}\frac{b_n}{(k_0 l)^2}\right)$$

In the present paper, the ground is supposed to be rigid. The number of modes, N, depends upon the propagation distance $r^\star$ into the shadow zone. As $r^\star$ is increased, the high-frequency content of the pressure wave is attenuated, and a smaller number of modes is necessary to compute the analytical expression. In the present study, a number of $N = 5000$ modes is used for the shortest distance (close to the cutoff), and a number of $N = 2$ modes is enough for the longest propagation distance into the shadow zone. The analytical expression is computed frequency by frequency, and an inverse Fourier transform is used to obtain the pressure waveform in the time domain.

Acknowledgments

This work was performed within the framework of the Labex CeLyA of Université de Lyon, operated by the French National Research Agency (ANR-10-LABX-0060/ANR-11-IDEX-0007). The authors would like to express their most sincere thanks to Jean-Michel Perrin and Pascal Souchotte for their help in setting up the experiment.

References

[1] Bradley, K. A., Hobbs, C. M., Wilmer, C. B., Sparrow, V. W., Stout, T. A., Morgenstern, J. M., Underwood, K. H., Maglieri, D. J., Cowart, R. A., Collmar, M. T., et al., "Sonic Booms in Atmospheric Turbulence (SONICBAT): The Influence of Turbulence on Shaped Sonic Booms," NASA CR-220509, NASA Armstrong Flight Research Center, April 2020, https://ntrs.nasa.gov/citations/20200002482.

[2] Honda, M., and Yoshida, K., "D-SEND#2 Flight Demonstration for Low Sonic Boom Design Technology," *28th Congress of the International Council of the Aeronautical Sciences*, Optimage Ltd., Sept. 2012, https://www.icas.org/ICAS_ARCHIVE/ICAS2012/PAPERS/941.PDF.

[3] Kanamori, M., Takahashi, T., Naka, Y., Makino, Y., Takahashi, H., and Ishikawa, H., "Numerical Evaluation of Effect of Atmospheric Turbulence on Sonic Boom Observed in D-SEND#2 Flight Test," *55th AIAA Aerospace Sciences Meeting*, AIAA Paper 2017-0278, Jan. 2017. https://doi.org/10.2514/6.2017-0278

[4] Page, J. A., and Loubeau, A., "Aircraft Noise Generation and Assessment Section 5—Overall Vehicle System Noise, Part *d*—Sonic Boom," *CEAS Aeronautical Journal*, Vol. 10, No. 1, 2021, pp. 335–353. https://doi.org/10.1007/s13272-019-00379-0

[5] Coulouvrat, F., "Sonic Boom in the Shadow Zone: A Geometrical Theory of Diffraction," *Journal of the Acoustical Society of America*, Vol. 111, No. 1, 2002, pp. 499–508. https://doi.org/10.1121/1.1371973

[6] Lonzaga, J. B., Page, J. A., Downs, R. S., Kaye, S. R., Shumway, M. J., Loubeau, A., and Doebler, W. J., "PCBoom Version 7 Technical Reference," NASA TM 20220007177, NASA Langley Research Center, Dec. 2022, https://ntrs.nasa.gov/citations/20220007177.

[7] Maglieri, D. J., Bobitt, P. J., Plotkin, K. J., Shepperd, K. P., Coen, P. G., and Richwine, D. M., "Sonic Boom, Six Decades of Research," NASA SP 20150006843, NASA Langley Research Center, Dec. 2014, https://ntrs.nasa.gov/citations/20150006843.

[8] Plotkin, K. J., Page, J., and Haering, E., "Extension of PCBoom to Over-the-Top Booms, Ellipsoidal Earch, and Full 3-D Ray Tracing," *13th AIAA/CEAS Aeroacoustics Conference*, AIAA Paper 2007-3677, May 2007. https://doi.org/10.2514/6.2007-3677

[9] Emmanuelli, A., Dragna, D., Ollivier, S., and Blanc-Benon, P., "Characterization of Topographic Effects on Sonic Boom Reflection by Resolution of the Euler Equations," *Journal of the Acoustical Society of America*, Vol. 149, No. 4, 2021, pp. 2437–2450. https://doi.org/10.1121/10.0003816

[10] Emmanuelli, A., Dragna, D., Ollivier, S., and Blanc-Benon, P., "Sonic Boom Propagation over Real Topography," *Journal of the Acoustical Society of America*, Vol. 154, No. 1, 2023, pp. 16–27. https://doi.org/10.1121/10.0019938

[11] Pierce, A. D., *Acoustics: An Introduction to Its Physical Principles and Applications*, 3rd ed., Acoustical Soc. of America Press, New York, 2019. https://doi.org/10.1007/978-3-030-11214-1

[12] Don, C. G., and Cramond, A. J., "Creeping Wave Analysis of Impulse Propagation Through a Shadow Boundary," *Journal of the Acoustical Society of America*, Vol. 80, No. 1, 1986, pp. 302–305. https://doi.org/10.1121/1.394146

[13] Don, C. G., and Cramond, A. J., "Comparison of Ray and Wave Approaches to Acoustic Impulse Propagation Prior to a Shadow Boundary," *Journal of the Acoustical Society of America*, Vol. 87, No. 3, 1990, pp. 1017–1025. https://doi.org/10.1121/1.398828

[14] Berry, A., and Daigle, G. A., "Controlled Experiments of the Diffraction of Sound by a Curved Surface," *Journal of the Acoustical Society of America*, Vol. 83, No. 6, 1988, pp. 2047–2058. https://doi.org/10.1121/1.396385

[15] Daigle, G. A., and Raspet, R., "Dispersion of Impulse Sound Above a Curved Surface," *Journal of the Acoustical Society of America*, Vol. 89, No. 1, 1991, pp. 101–106. https://doi.org/10.1121/1.400514

[16] Pridmore-Brown, D. C., and Ingard, U., "Sound Propagation into the Shadow Zone in a Temperature-Stratified Atmosphere Above a Plane Boundary," *Journal of the Acoustical Society of America*, Vol. 27, No. 1, 1955, pp. 36–42. https://doi.org/10.1121/1.1907493

[17] Maglieri, D. J., "Sonic Boom Flight Research—Some Effects of Airplane Operations and the Atmosphere on Sonic Boom Signatures," *Journal of the Acoustical Society of America*, Vol. 39, No. 5B, 1966, pp. 36–42. https://doi.org/10.1121/1.1914042

[18] Cheinet, S., Cosnefroy, M., Königstein, F., Rickert, W., Christoph, M., Collier, S. L., Dagallier, A., Ehrhardt, L., Ostashev, V. E., Stefanovic, A., et al., "An Experimental Study of the Atmospheric-Driven Variability of Impulse Sounds," *Journal of the Acoustical Society of America*, Vol. 144, No. 2, 2018, pp. 822–840. https://doi.org/10.1121/1.5047750

[19] Crow, S. C., "Distortion of Sonic Bangs by Atmospheric Turbulence," *Journal of Fluid Mechanics*, Vol. 37, No. 3, 1969, pp. 529–563. https://doi.org/10.1017/S0022112069000711

[20] Plotkin, K. J., Maglieri, D. J., and Sullivan, B. S., "Measured Effects of Turbulence on the Loudness and Waveforms of Conventional and Shaped Minimized Sonic Booms," *11th AIAA/CEAS Aeroacoustics Conference*, AIAA Paper 2005-2949, May 2005. https://doi.org/10.2514/6.2005-2949

[21] Raspet, R., Bass, H. E., Yao, L., Boulanger, P., and McBride, W. E., "Statistical and Numerical Study of the Relationship Between Turbulence and Sonic Boom Characteristics," *Journal of the Acoustical Society of America*, Vol. 96, No. 6, 1994, pp. 3621–3626. https://doi.org/10.1121/1.410579

[22] Auger, T., and Coulouvrat, F., "Numerical Simulation of Sonic Boom Focusing," *AIAA Journal*, Vol. 40, No. 9, 2002, pp. 1726–1734. https://doi.org/10.2514/2.1877

[23] Downs, R. S., Kaye, S., and Page, J. A., "Sonic Boom Prediction Workshop 3: Propagation Modeling Using PCBoom," AIAA Paper 2020-2760, June 2020. https://doi.org/10.2514/6.2020-2760

[24] Zelias, A., Gainville, O., and Coulouvrat, F., "Complex Ray Analytical Solutions for Infrasound and Sonic Boom Propagation into Shadow Zones," *Forum Acusticum 2020*, Lyon, France, Dec. 2020, https://doi.org/10.48465/fa.2020.0240

[25] Cheinet, S., Ehrhardt, L., Juvé, D., and Blanc-Benon, P., "Unified Modeling of Turbulence Effects on Sound Propagation," *Journal of the Acoustical Society of America*, Vol. 132, No. 4, 2012, pp. 2198–2209. https://doi.org/10.1121/1.4748584

[26] Carr, A. N., Lonzaga, J. B., and Miller, S. A., "Numerical Prediction of Loudness Metrics for *N*-Waves and Shaped Sonic Booms in Kinematic Turbulence," *Journal of the Acoustical Society of America*, Vol. 151, No. 6, 2022, pp. 3580–3593. https://doi.org/10.1121/10.0011514

[27] Carr, A. N., Lonzaga, J. B., and Miller, S. A., "Split-Step Simulations to Assess the Effects of Atmospheric Boundary Layer Turbulence on the Dose Variability of *N*-Waves and Shaped Booms," *Journal of Sound and Vibration*, Vol. 571, 2024, Paper 118118. https://doi.org/10.1016/j.jsv.2023.118118

[28] Kanamori, M., Takahashi, T., Ishikawa, H., Makino, Y., Naka, Y., and Takahashi, H., "Numerical Evaluation of Sonic Boom Deformation Due to Atmospheric Turbulence," *AIAA Journal*, Vol. 59, No. 3, 2021, pp. 972–986. https://doi.org/10.2514/1.J059470

[29] Leconte, R., Chassaing, J., Coulouvrat, F., and Marchiano, R., "Propagation of Classical and Low Booms Through Kinematic Turbulence with Uncertain Parameters," *Journal of the Acoustical Society of America*, Vol. 151, No. 6, 2022, pp. 4207–4227. https://doi.org/10.1121/10.0011771

[30] Lonzaga, J. B., "Multiple Scattering Theory for Modeling Sonic Booms in Atmospheric Turbulence," *Journal of the Acoustical Society of America*, Vol. 154, No. 5, 2023, pp. 3078–3088. https://doi.org/10.1121/10.0022385

[31] Stout, A. T., Sparrow, V. W., and Blanc-Benon, P., "Evaluation of Numerical Predictions of Sonic Boom Level Variability due to Atmospheric Turbulence," *Journal of the Acoustical Society of America*, Vol. 149, No. 5, 2021, pp. 3250–3260. https://doi.org/10.1121/10.0004985

[32] Luquet, D., Marchiano, R., and Coulouvrat, F., "Long Range Numerical Simulation of Acoustical Shock Waves in a 3D Moving Heterogeneous and Absorbing Medium," *Journal of Computational Physics*, Vol. 379, 2019, pp. 237–261. https://doi.org/10.1016/j.jcp.2018.11.041

[33] Sanai, M., Toong, T. Y., and Pierce, A. D., "Ballistic Range Experiments on Superbooms Generated by Refraction," *Journal of the Acoustical Society of America*, Vol. 59, No. 3, 1976, pp. 513–519. https://doi.org/10.1121/1.380907

[34] Almgren, M., "Simulation by Using a Curved Ground Scale Model of Outdoor Sound Propagation Under the Influence of a Constant Sound Speed Gradient," *Journal of Sound and Vibration*, Vol. 118, No. 2, 1987, pp. 353–370. https://doi.org/10.1016/0022-460X(87)90531-1

[35] Qin, Q., Attenborough, K., Ollivier, S., and Blanc-Benon, P., "Effects of Surface Roughness and Turbulence on Propagation of Shock Waves Above a Curved Surface," *11th International Symposium on Long Range Sound Propagation*, Fairlee, June 2004.

[36] Wasier, J., "Étude expérimentale des effets d'une frontière sur la propagation des ondes acoustiques à travers une turbulence thermique (Experimental Study of the Acoustical Propagation Through Thermal Turbulence with a Boundary)," Ph.D. Dissertation, École Centrale de Lyon 99-46, 1999., France, 1999, https://acoustique.ec-lyon.fr/publi/wasier_thesis.pdf.

[37] Averiyanov, M., Ollivier, S., Khokhlova, V., and Blanc-Benon, P., "Random Focusing of Nonlinear Acoustic N-Waves in Fully Developed Turbulence: Laboratory Scale Experiment," *Journal of the Acoustical Society of America*, Vol. 130, No. 6, 2011, pp. 3595–3607. https://doi.org/10.1121/1.3652869

[38] Ganjehi, L., Marchiano, R., Coulouvrat, F., and Thomas, J., "Evidence of Wave Front Folding of Sonic Booms by a Laboratory-Scale Deterministic Experiment of Shock Waves in a Heterogeneous Medium," *Journal of the Acoustical Society of America*, Vol. 124, No. 1, 2008, pp. 57–71. https://doi.org/10.1121/1.2832621

[39] Lipkens, B., and Blackstock, D. T., "Model Experiment to Study Sonic Boom Propagation Through Turbulence. Part I. General Results," *Journal of the Acoustical Society of America*, Vol. 104, No. 3, 1998, pp. 1301–1309. https://doi.org/10.1121/1.424339

[40] Ollivier, S., and Blanc-Benon, P., "Model Experiment to Study Acoustic *N*-Wave Propagation Through Turbulence," *10th AIAA/CEAS Aeroacoustics Conference*, AIAA Paper 2004-2921, May 2004. https://doi.org/10.2514/6.2004-2921

[41] Salze, E., Yuldashev, P., Ollivier, S., Khokhlova, V., and Blanc-Benon, P., "Laboratory-Scale Experiment to Study Nonlinear *N*-Wave Distortion by Thermal Turbulence," *Journal of the Acoustical Society of America*, Vol. 136, No. 2, 2014, pp. 556–566. https://doi.org/10.1121/1.4887458

[42] Willis, W. A., Valdez, J. A., Pineau, P., Bogey, C., Tinney, C. E., and Hamilton, M. F., "A Study of Mach Wave Coalescence Using Spark Sources and Large-Eddy Simulation," *AIAA SciTech 2023 Forum*, AIAA Paper 2023-0021, Jan. 2023. https://doi.org/10.2514/6.2023-0021

[43] Wright, W., "Propagation in Air of *N*-Waves Produced by Sparks," *Journal of the Acoustical Society of America*, Vol. 73, No. 6, 1983, pp. 1948–1955. https://doi.org/10.1121/1.389585

[44] Yuldashev, P. V., Averiyanov, M. V., Khokhlova, V. A., Ollivier, S., and Blanc-Benon, P., "Nonlinear Spherically Divergent Shock Waves Propagating in a Relaxing Medium," *Acoustical Physics*, Vol. 54, No. 1, 2008, pp. 32–41. https://doi.org/10.1134/S1063771008010065

[45] Yuldashev, P. V., Ollivier, S., Averiyanov, M., Sapozhnikov, O., Khokhlova, V., and Blanc-Benon, P., "Nonlinear Propagation of Spark-Generated *N*-Waves in Air: Modeling and Measurements Using Acoustical and Optical Methods," *Journal of the Acoustical Society of America*, Vol. 128, No. 6, 2010, pp. 3321–3333. https://doi.org/10.1121/1.3505106

[46] Yuldashev, P. V., Karzova, M. M., Khokhlova, V. A., Ollivier, S., and Blanc-Benon, P., "Mach-Zehnder Interferometry Method for Acoustic Shock Wave Measurements in Air and Broadband Calibration of Microphones," *Journal of the Acoustical Society of America*, Vol. 137, No. 6, 2015, pp. 3314–3324. https://doi.org/10.1121/1.4921549

[47] Cotté, B., and Blanc-Benon, P., "Estimates of the Relevant Turbulent Scales for Acoustic Propagation in an Upward Refracting Atmosphere," *Acta Acoustica United with Acustica*, Vol. 93, 2007, pp. 944–958, https://dael.euracoustics.org/bin/EAA/v2.60/quickview?id=64574.

[48] Darden, C. M., Powell, C. A., Hayes, W. D., George, A. R., and Pierce, A. D., "Status of Sonic Boom Methodology and Understanding", "Status of Sonic Boom Methodology and Understanding," NASA CP 3027, Jan. 1988, https://ntrs.nasa.gov/citations/19890014044.

[49] Blanc-Benon, P., and Juvé, D., "Intensity Fluctuations of Spherical Acoustic Waves Propagating Through Thermal Turbulence," *Waves in Random Media*, Vol. 3, No. 2, 1993, pp. 71–83. https://doi.org/10.1088/0959-7174/3/2/002

[50] Averiyanov, M., Blanc-Benon, P., Cleveland, R., and Khokhlova, V., "Nonlinear and Diffraction Effects in Propagation of *N*-Waves in Randomly Inhomogeneous Moving Media," *Journal of the Acoustical Society of America*, Vol. 129, No. 4, 2011, pp. 1760–1772. https://doi.org/10.1121/1.3557034

[51] Chevret, P., Blanc-Benon, P., and Juvé, D., "A Numerical Model for Sound Propagation Through a Turbulent Atmosphere Near the Ground," *Journal of the Acoustical Society of America*, Vol. 100, No. 6, 1996, pp. 3587–3599. https://doi.org/10.1121/1.417224

[52] Herbert, G., Hass, W., and Angell, J., "A Preliminary Study of Atmospheric Effects on the Sonic Boom," *Journal of Applied Meteorology*, Vol. 8, 1969, pp. 618–626. https://doi.org/10.1175/1520-0450(1969)008

[53] Salze, E., Ollivier, S., Blanc-Benon, P., Yuldashev, P., and Khokhlova, V., "Characterisation of the Sound Field Emitted by a Electric Spark Source in Air," *Forum Acusticum 2011*, Aalborg, Denmark, June 2011, https://acoustique.ec-lyon.fr/publi/salze_acusticum11.pdf.

[54] George, A., and Plotkin, K., "Propagation of Sonic Booms and Other Weak Nonlinear Waves Through Turbulence," *Physics of Fluids*, Vol. 14, No. 3, 1971, pp. 548–554. https://doi.org/10.1063/1.1693471

[55] Pierce, A., "Statistical Theory of Atmospheric Turbulence Effects on Sonic-Boom Rise Times," *Journal of the Acoustical Society of America*, Vol. 49, No. 3B, 1972, pp. 906–929. https://doi.org/10.1121/1.1912431

[56] Niedzwiecki, A., and Ribner, H., "Subjective Loudness of N-Wave Sonic Boom," *Journal of the Acoustical Society of America*, Vol. 64, No. 6, 1978, pp. 1617–1621. https://doi.org/10.1121/1.382146

L. Ukeiley
Associate Editor